



CdS nanowires encapsulated liquid crystal in-plane switching of LCD device

Kaushik Pal¹ · M. Abd Elkodous² · M. L. N. Madhu Mohan³

Received: 20 March 2018 / Accepted: 10 April 2018 / Published online: 16 April 2018
© Springer Science+Business Media, LLC, part of Springer Nature 2018

Abstract

Well-defined ultra-thin ‘wire’ like cadmium sulfide (CdS) nanostructures have been synthesized by applying simple cost-effective hydrothermal route. The content of nanostructures modifies the nature of surface interaction between two liquid crystal (LC) components as revealed by optical and electrical investigation. Those synthesized nanowires have an average diameter of about 7–10 nm and length up to several micrometers region. A possible mechanism has been proposed and the addition of cataionic surfactant cetyltrimethylammonium bromide (CTAB) into the two mixed-solvents would play an important role on the growth dynamics of the desired product. Those CdS-nanowires dispersing LC was found a remarkable signature on the nucleation and provides a more fundamental approach to modify the crystallographic configuration of host nanostructures. Polarizing optical microscopy (POM) revealed temperature dependent various phases appearance in different textural patterns are the proof the significant influence of CdS nanomaterials complete homogenous dispersion with host LC-matrix. Most observed phenomena are discussed in terms of a new smectic ordering labeled as ‘Smectic X*’, which is sandwiched between the traditional ‘Nematic’ and convectional ‘Smectic C*’ phases. This feature article deals with dielectric relaxations, rotational viscosity, spontaneous polarization in the smectic C phase have been analyzed. A range of remarkable responses of the capacitance with voltage in a Preisach model, fourfold dipolar species in hybrid nanocomposites matrix as well as bi-stable DC switching also offering recent breakthroughs in next generation smart display (LCD) and novel switchable device.

1 Introduction

A high yield novel semiconductor nanostructure has attracted much attention in recent years due to their unusual optical and electrical properties [1, 2]. As one of the most important II–VI group semiconductors, CdS nanocrystals have critical application in solar cells, non-linear optical, quantum size effect semiconductors, optoelectronic and

electronic devices [3, 4]. Very late, considerable progress has been made in the synthesis of 1-D CdS nanostructures. For instance, Pal’s group reported last decades several chemical assisted routes based on unique hydrothermal strategy for preparing morphologies of CdS nanowires and nanorods [5–7]. Liquid crystals (LC) have revolutionized the smart display and communication technologies. Doping of LC with inorganic nanoparticles such as: carbon-nanotubes, gold-nanoparticles and ferroelectric nanoparticles have garnered the interest of research community as they aid in improving the electro-optic performance.

Moreover, Pal’s co-workers employed many technological applications of nanomaterials are intentionally ‘dispersed’ by introducing appropriate amounts of foreign elements (liquid crystal) into hosts to impart electronic, optical, electro-optical switching properties [8]. Recently, keeping in pace with topical science, novel hydrogen bonded liquid crystals have entered into the fascinating domains of ‘Liquid Crystal Nanoscience (LCN)’ [9–11]. One of the most recent syntheses of hydrogen-bonded liquid crystals (HBLCs) are relatively easier than that of conventional LC and have the potential for

✉ Kaushik Pal
kaushikphysics@gmail.com;
kaushikpaul.nano@bharathuniv.ac.in

¹ Department of Nanotechnology, Bharath Institute for Higher Education and Research (BIHER) Research Park, Bharath University, 173 Agharam Road, Selaiyur, Chennai, Tamil Nadu 600073, India

² School of Engineering and Applied Sciences, Center for Nanotechnology (CNT), Nile University, Sheikh Zayed, Giza, Egypt

³ Liquid Crystal Research Laboratory (LCRL), Bannari Amman Institute of Technology, Sathyamangalam 638 401, India

developing optical properties by smooth dispersion of nanomaterials [12, 13]. Hydrogen bonded liquid crystal complexes have attracted a great deal of interest, due to their structural and dynamic properties as they play significant roles in many chemical and biological systems [14, 15]. By choosing an appropriate proton acceptor and proton donor, stable intermolecular hydrogen bonds can be formed and thereby they provide a novel system with new properties [16–18]. In fact, in this feature article it is highly desirable to seek a facile and effective methodology for the synthesis of CdS nanowires dispersing liquid crystal is the best response compared to pure LC composite. The most recent efforts are mainly providing an overview idea of the current progresses in doping-induced control of crystallographic phase structures, sizes, shapes, as well as performances of functional nanomaterials for the latest approach. However, frequency variation dielectric relaxation responses, spontaneous polarization, rotational viscosity are the significant commercial application in smart switchable capacitor demands further improvements of the physical properties of the CdS nanowires blended HBLC to yield better electrical response with lower driving voltage, and good alignment without chevron structures.

2 Experimental details

2.1 Materials and methods

Starting materials were used in this investigation were analytical grade, commercially available and received without further purification (99.5%). Cadmium acetate [$\text{Cd}(\text{CH}_3\text{COO})_2$], ethylene diamine (EDA), and cataionic surfactant cetyltrimethylammonium bromide [CTAB; $(\text{C}_{19}\text{H}_{42}\text{BrN})$], were used as starting ingredients for synthesis of various nano-structured molecules. Hydrogen bonded liquid crystal compounds were composed of azelaic acid with p-n-pentyloxy and heptyloxy benzoic acids (AC + 5BAO; AC + 7BAO) supplied by Sigma-Aldrich, (Germany). *N,N*-dimethyl formamide (DMF) and other solvents were purchased in high performance liquid chromatography (HPLC) grade and used as received. Typical hydrothermal methodology employed and the speed of centrifugation were controlled at 6000 rpm to obtain CdS nanostructures. All desired nanomaterials and hybrid LC compounds were purified (95%) by N_2 gas flow and rest proton extracted by slight heating in a regular laboratory electric oven.

2.2 CdS nanowires fabrication

Briefly, in our typical approach to generate ultra-thin CdS nanowires is based on the premise that surfactant mixtures may generate templates novel growth dynamics. In a typical procedure, 0.33 gm of cadmium acetate [$\text{Cd}(\text{CH}_3\text{COO})_2$] with equimolar amount of sulfur powder (S) mixed in a container. A 60 cm^3 aqueous solution of final pH 7 containing ethylene diamine (3 mmol) was added into a container and left for vigorous stirring and obtained lime yellow solution. This solution transferred into a Teflon lined autoclave (100 ml) and injected the hot stock solution of 1.0 m Mole amount of cetyltrimethylammonium bromide (CTAB) surfactant was maintained until dark yellow at 100 °C for 24 h, and then cooled naturally in air. The resulting precipitates collected by centrifugal separation were washed with several times deionized water (DIW) and absolute ethanol and then dried one time under vacuum for 20 h at 40 °C. The desired ‘powder’ like samples were allowed to dry for several times with the continuous flow of nitrogen (N_2) gas.

2.3 Preparation of HBLC

A specific, HBLC is composed of azelaic acid with p-n-pentyloxy and heptyloxy benzoic acids (AC + 5BAO) & (AC + 7BAO) utilized for hybrid compounds. Intermolecular double hydrogen bonded mesogens were synthesized by the addition of 2.5 mol of p-n-alkoxybenzoic acids (nOBA) with 1.2 mol of azelaicdicarboxylic acid into *N,N*-Dimethyl formamide (DMF). Further, they were taken subject to constant stirring for 10 h at ambient temperature (45 °C) until a white precipitate in a dense solution is formed. The white crystalline crude complexes were obtained by removing excess DMF are recrystallized with dimethyl sulfoxide (DMSO) and the yield varied from 80% to 95%. The formation of multimer is avoided by recrystallization of the product. The original chemical formula of liquid crystals comprising azelaic acid (AC) with p-n-alkyloxy benzoic acid (nBAO) by varying the respective alkyloxy carbon number ($n=5$ and $n=7$) as follows in Fig. 1a and b respectively.

Also, the molecular dynamics protocols are commonly utilized in studying hydrogen bonded liquid crystal (AC + nBAO) by simulation along with the atomic numbering scheme of all the hydrogen bonded mesogens corresponds to (X + nBAO) series, where X = AC; when $m=7$ for AC and, carbon numbers variations $n=5$ to 7.

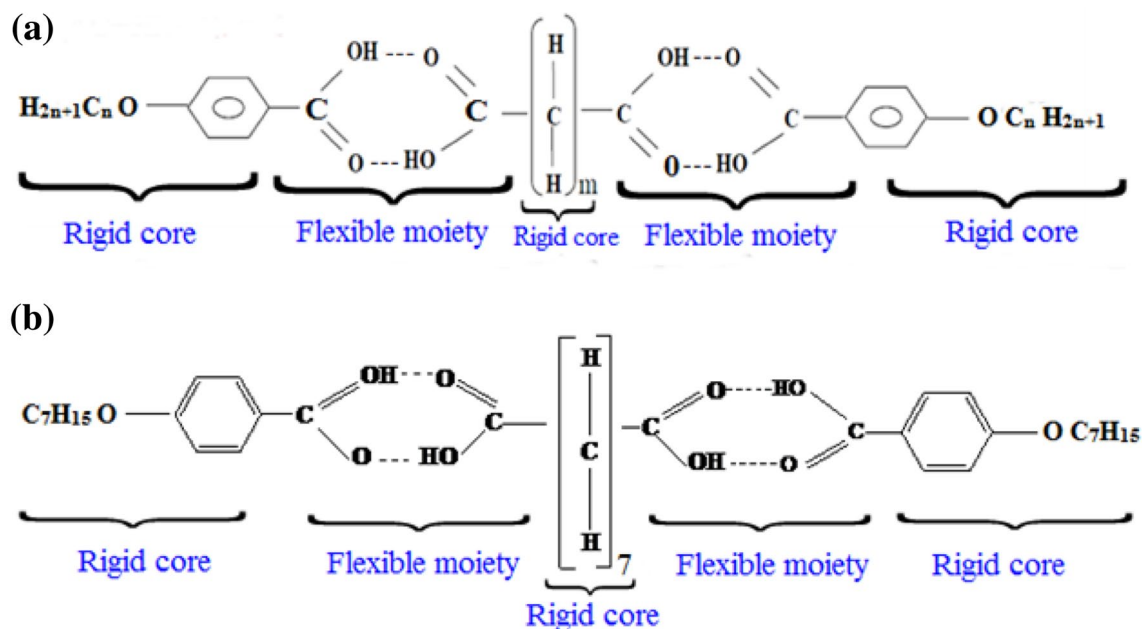
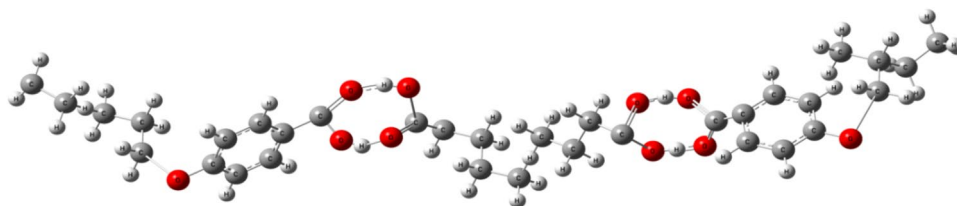


Fig. 1 Chemical formula of intermolecular double hydrogen bonded mesogens of liquid crystal's series of **a** azelaic acid (AC) combined p-n-pentyloxy benzoic acid (AC+5BAO), and **b** azelaic acid (AC) combined p-n-heptyloxy benzoic acid (AC+7BAO)



2.4 Nanomaterials dispersed liquid crystal (NDLC) nanocomposite sample preparation

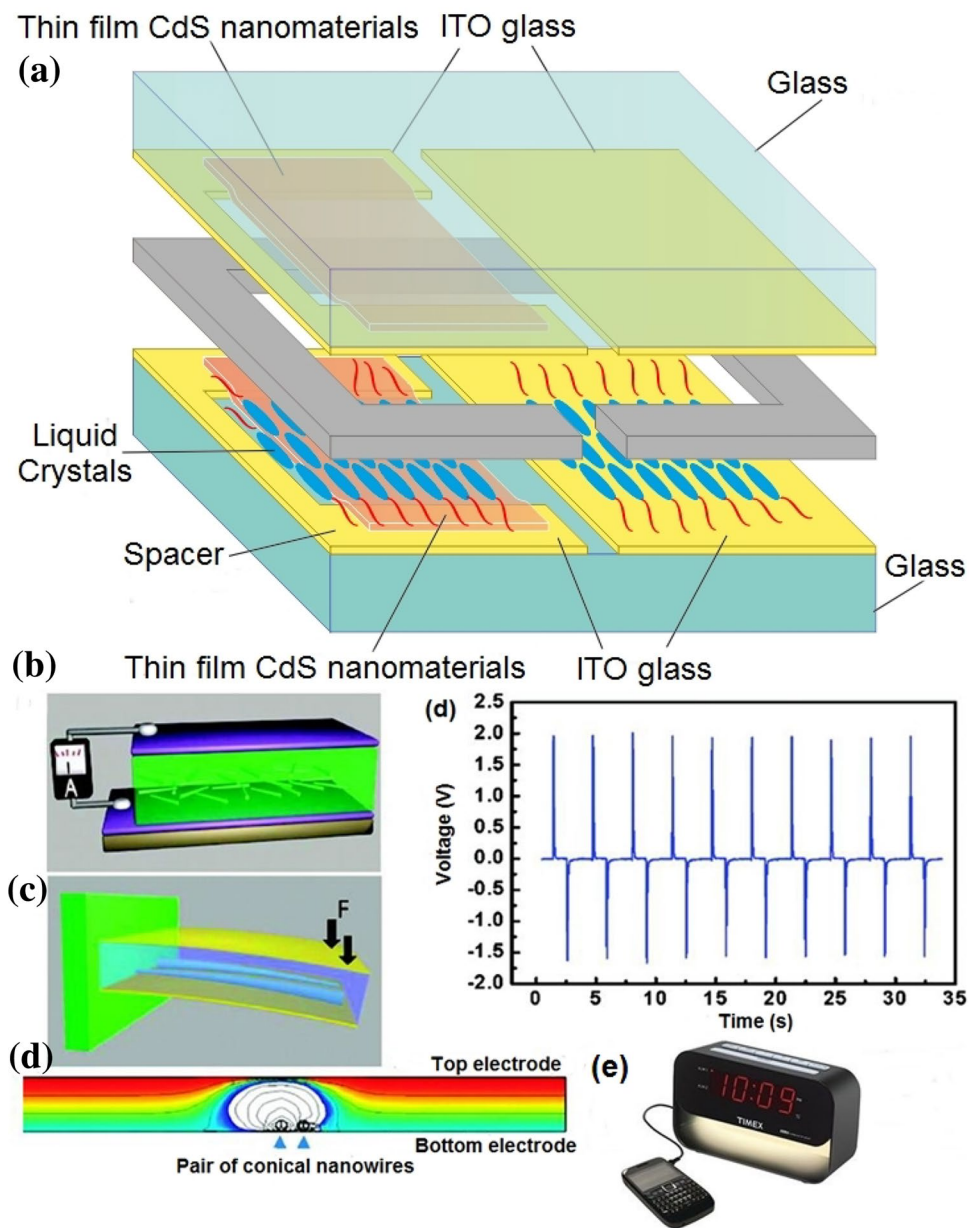
Typical amounts (0.235 gm) of as-synthesized CdS nanomaterials were combined with 0.007% as-prepared pure liquid crystals suspension. The solution was vigorously stirred during 1.5 h, followed by ultrasound vibration for smooth dispersion. After that, the deposition was collected and vacuum dried at 50 °C for 4 h, which has the function of facilitating the combination of the CdS nanomaterials dispersed with liquid crystal compounds.

2.5 Modulation of liquid crystal nanocomposite device

Commercial electro-optical LC cells with ITO electrodes (electrode area: 4 × 4 mm²) and alignment layers were deposited on the inner surface of the confining substrates; the alignment layers were rubbed in unidirectional and assembled in an anti-parallel fashion with respect to the rubbing directions for a planar alignment. The cell gap was

maintained with 1.0 μm spacer placed between the substrates. This free cell is placed into hot plate under treatment of (2 °C/min). NDLC samples were distributed inside heated cells by flow of capillary action. Suspensions were fabricated in this way were then put into photo-refractive ITO-LC cell. The thickness of the photo-refractive test cell was about 0.1 μm, thin enough to allow surface stabilization of the specimen. The schematic representation of the development to create a CdS nanomaterials-incorporated liquid crystal of surface stabilized electrically sensible switchable device performance with NDLC samples confined geometry on an ITO–ITO structure, as shown in the Fig. 2a. Moreover, in the bottom images in Fig. 2b–e are basically are operated by external voltages employed, which are favourable power consumption characteristics to the piezoelectric energy harvester without the need for a high current supply. Due to the typical geometrical shape of photo refractive ITO–LC cell, the nanowires are assembled with a unipolar feature, which is probably the key for producing a macroscopic piezoelectric potential in the direction normal to the substrate. This harvester produced output voltage up to 2 V (an equivalent

Fig. 2 **a** A graphical representation of the CdS nanowires dispersed hydrogen bonded liquid crystals (HBLCs) composite matrix confined geometry into conducting ITO–LC cell electro-optical switching was performed by LCD device, **b** a schematic image of the fabricated energy harvester using CdS nanowires; **c** a model showing the set up for measuring the energy conversion. The polyimide substrate used to hold the nanogenerator at its upper side, where the force ‘F’ is applied. The CdS-NW’s are under compressive strain during the deformation; **d** the model used for calculating the potential distribution across the top and bottom electrodes of the harvester with the presence of a pair of CdS-NW’s, and **e** the measured output voltage, and smart technology of LCD panel display driven by the harvester



open circuit voltage of 3.3 V) with a few hundreds of nano amperes of output current, which can drive a small LCD panel.

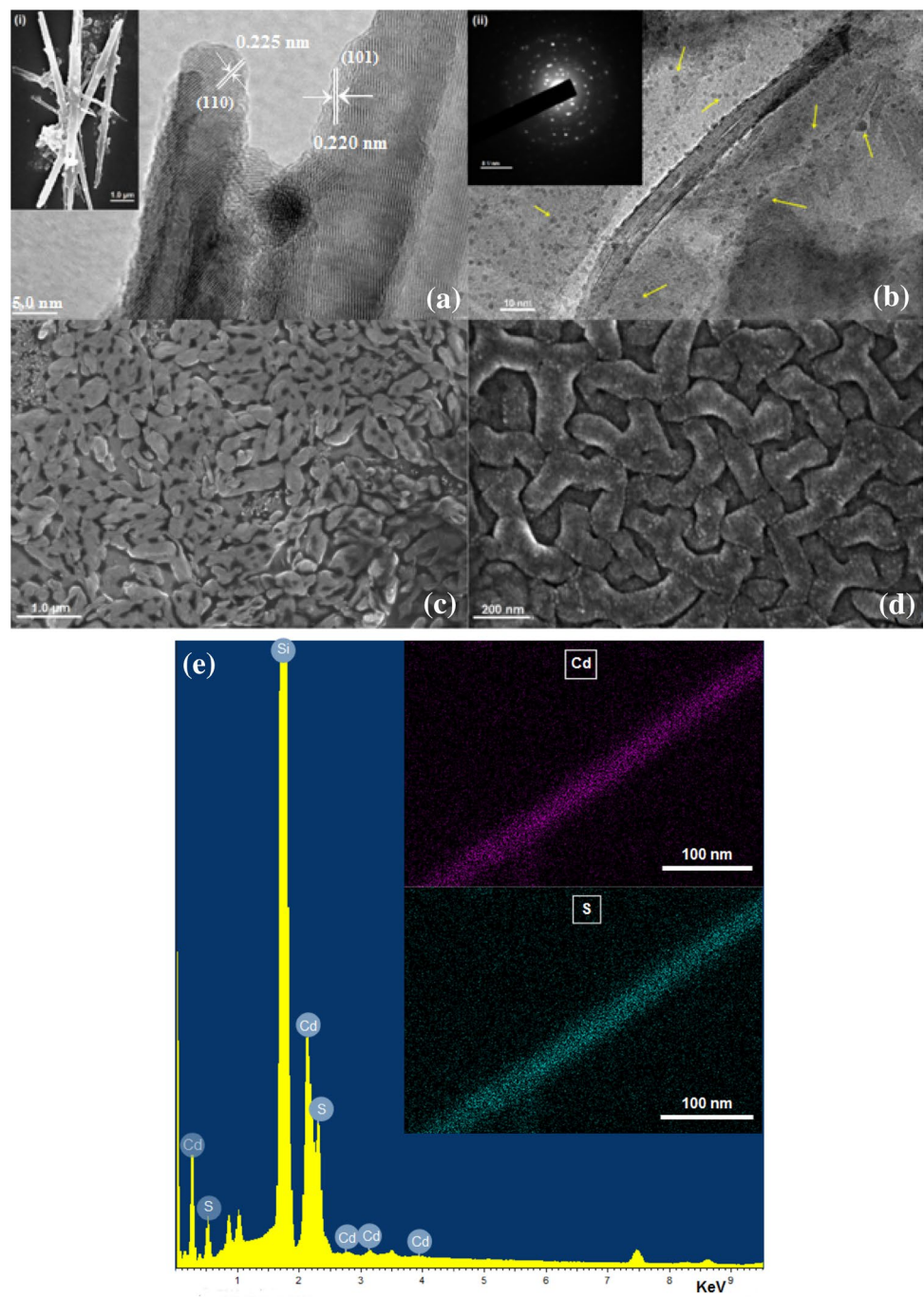
3 Results and discussions

The CdS-nanowires were prepared on a large scale. The morphology and dimension of the product were examined by FE-SEM [Inset (i): Fig. 3a] and HR-TEM. Figure 3a illustrates the typical HR-TEM image of the product. To evaluate the morphology of CdS-nanowires thin-film cross-sectional images of the samples were precisely observed by using a Transmission Electron Microscopy (TEM) JEOL JEM-2100

(HR). The HR-TEM samples were sliced to a thickness of tens of nm perpendicular to the carbon coated copper grid at an acceleration voltage of 200 kV. Moreover, the SAED patterns and high-angle annular dark field scanning HR-TEM (ORIOUS™ SC 1000 CCD) images were also obtained for crystalline analysis and Z-contrast imaging.

It can be seen that, the product is composed of uniform nanowires with an average diameter of 7–10 nm and length up to the several micro meter range. The image demonstrates that CdS-nanowires with a small thickness and a high aspect ratio can be readily prepared by the present method depicted individual nanowires, which was also confirmed by field emission scanning electron microscopy (FE-SEM, SIGMA ZEISS) image Fig. 3b. The clear crystal lattice fringes

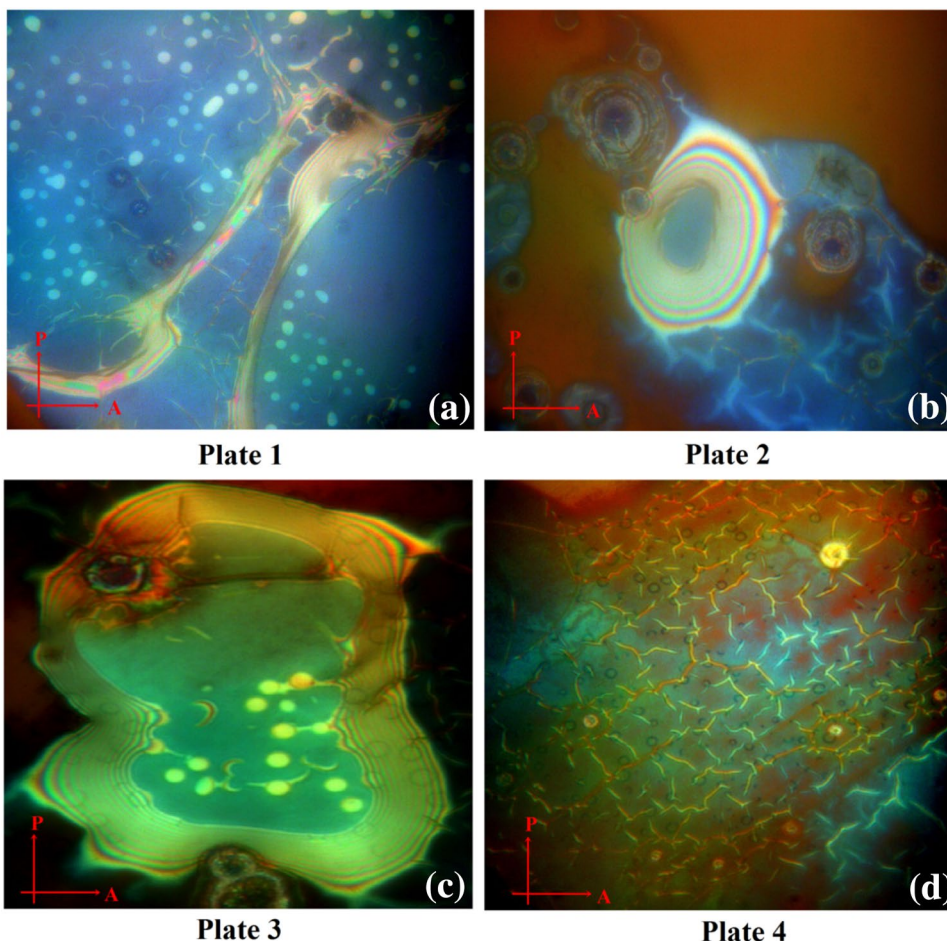
Fig. 3 Typical high resolution transmission electron microscopic (HR-TEM) image of as-prepared **a** CdS nanowires [Inset: (i) FE-SEM morphology], **b** liquid crystal (highlighted by ‘yellow’ arrow) dispersed on CdS-nanowires HR-TEM image [Inset: (ii) SEAD pattern of nanomaterials dispersed liquid crystals polycrystalline structure], **(c)** ‘worm’ like FE-SEM image of liquid crystal (AC + 5BAO), and **d** netted ‘worm’ like FE-SEM image of liquid crystal (AC + 7BAO), **e** distribution peaks of chemical composition by EDS pattern [Inset: Cadmium (Cd) and sulfur (S) element confirmation into the precursor system by chemical mapping]. (Color figure online)



demonstrate that, the nanowires are well crystallized. Furthermore, the HR-TEM image reveals that, the average interplanar distance along the growth axis is 0.220 nm, which is consistent with the interplanar distance of the (101) plane of the wurtzite structure of CdS, thus confirming that the nanowires are elongated along the *c*-axis. However, small black spots are prominently shown between two sides of semiconductor CdS-nanowires resulted in Fig. 3b is due to LC compounds (indicated by ‘yellow’ arrow). The SAED pattern [Inset (ii) of Fig. 3b] consists of broad diffuse rings,

further confirming the poly crystalline nature of the fabricated CdS nanowires. Moreover, prominent ‘worm’ like morphologies were observed, particularly for hydrogen bonded liquid crystals (AC + 5BAO) and (AC + 7BAO) depicted in Fig. 3c, and d respectively. However, energy dispersion spectrometer (EDS) were analyzed corresponding to the peak distribution of chemical elements of typical percentages (Cd—86.5% and S—13.7%) as shown in the Fig. 3e, ensures CdS-nanowires and the percentage of chemical elements were detected by chemical mapping

Fig. 4 Collection of typical texture patterns of optical micrograph under cross polarizer with 20x magnification at temperature variance pure liquid crystals compound (AC + nBAO; $n=5$ and 7) series. **a** ‘Droplet’ texture of nematic (N) phase at 140 °C (Plate 1), **b** threaded round orbital nematic schlieren texture (Plate 2), **c** netted schlieren round orbital with nematic micro-droplets pattern (Plate 3), and **d** ‘worm’ like textural appearance due to smectic X^* phase at 113.8 °C (Plate 4)



analysis also shown inset image of Fig. 3e. This pattern verifies the high purity of as-prepared CdS nanowires were mixed with liquid crystals compound due to the formation of hybrid NDLC composite.

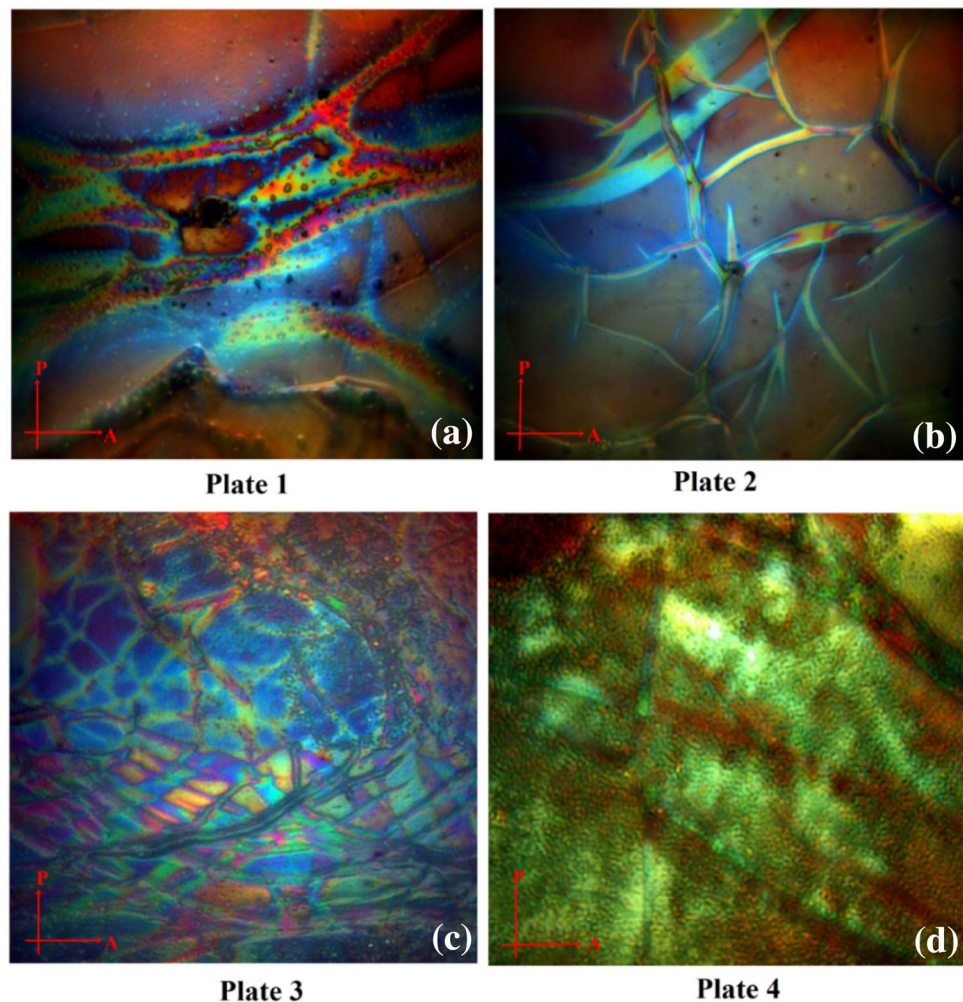
Surface stabilized smectic uniform lying helical texture and electro-optical switching with different temperature variation calculated by polarizing optical microscopy (Model: OLYMPUS, CX31, 6J09934 Japan) with a signal generator U8031A. Commercial electro-optical LC-cells with ITO electrode samples were distributed inside heated cells by flow of capillary action under cross polarizer. Molecular alignment and uniform textures were slowly developed as the LC isotropic temperature is allowed to cool down slowly due to perfect alignment of molecules at room temperature. Also, a small bias field is maintained to prevent cells for electro-optical (EO) switching. Phase variance and texture patterns with the planar boundary conditions study through POM ensures from crystal structure corresponding at temperature as shown in Fig. 4 (LC compounds). Those typical textural patterns are found to exhibit characteristic textures viz., nematic (N) phase of droplet texture appeared at 140 °C (Plate 1), threaded nematic schlieren texture with droplet (Plate 2), nematic schlieren orbital pattern (Plate 3), and

‘worm’ like textural appearance due to smectic X^* phase (Sm X^*) investigated at temperature 113.8 °C (Plate 4).

Hence, the homogenous dispersion of CdS nanowires with thermotropic hydrogen bonded liquid crystal (HBLC) nanocomposite displayed in Fig. 5. While, textural phase pattern certainly changes e.g. multi-colored nematic droplet at 138.2 °C (Plate 1), smooth multicolor leaf-net pattern of N phase (Plate 2), free standing mosaic pattern of Sm C^* phase appeared at 125 °C (Plate 3) and ‘worm’ like Sm X^* phase were identified between Sm C^* and N, at 112 °C (Plate 4), illustrated in details. The corresponding phase sequence of two LC composite as represented (Cr 60 Sm X^* 113.8 N 140 Iso 142.5) [19] and CdS-NW’s dispersed LC composite matrix (Cr 61.2 Sm X^* 112.2 Sm C^* 125 N 138.2 Iso 140).

The variation of relaxation frequency with capacitance in ‘Gold stone’ mode of covering the entire thermal span of Sm C^* corresponding to CdS nanomaterials, LC compounds and CdS-nanowires dispersed LC composite matrix as illustrated in Fig. 6a. It can be explored that, at the transition temperature of a Sm C^* phase region, the magnitude of the relaxation frequencies decreases and shifts to the lower side, which is in accordance with the reported data on ferroelectric liquid crystal (FLC). In fact, the suppression of

Fig. 5 Temperature dependence typical collection of textural phase studies by optical micrograph under cross polarizer with 20x magnification of CdS-nanowires dispersed liquid crystals composite matrix. **a** A multi-colored nematic micro droplet at 138.2 °C (Plate 1), **b** smooth multicolor leaf-net pattern of Nematic phase (Plate 2), **c** free standing mosaic pattern of Sm C* phase appeared at 125 °C (Plate 3), and **d** ‘worm’ like Sm X* phase identified at 112 °C (Plate 4)



dielectric relaxation with applied field has been noticed in entire Sm C* thermal span by plotting permittivity on X-axis against dielectric loss on Y-axis. The field and temperature variance of spontaneous polarization (P_s) through sample switching evidence as performed by a digital oscilloscope (Model: GW INSTEK, GDS-2302A equipped with triple output DC power supply KEYSIGHT U8031A, 0–30 V, 6 A/5 V, 3 A) as shown in Fig. 6b. Spontaneous polarization attains a saturated value, while near the transition point of temperature at 50–80 °C drastically increase corresponds to nanowires dispersed LC composite matrix, while it follows similar fashion quite shift peak intensity observed due to pure LC composite. It reveals the existences of ‘Sm C*’ and ‘N’ phases are ferroelectric phases. The suppression of the frequency with filed in both these phases have been noticed in pure LC composite. The formation of EDL around the nanowires screens the polarization director of the nanowires dispersed LC composite sample, which is one of the possible

reasons behind the molecular movement describing spontaneous polarization (P_s).

However, the behavior of the rotational viscosity shows similar characteristics to the polarization and its value lies between 125 and 2750 mN s m^{-2} , as shown in the Fig. 6c. By increasing temperature starts from 50 °C to the isotropic point we confirmed and detail investigation shows that, the rotation viscosity rapidly increases with a transition temperature significantly due to the increase of degrees of freedom of CdS-nanowires encapsulated LC composite matrix. Also, the relaxation frequency is higher in the incorporated LC composite cell due to the increase in the rotational viscosity. At room temperature the nanomaterial in the LC composite matrix is frozen due to the strong confinement (LC interactions become stronger) of the LC matrix. This confinement is increased due to the thermal energy and the rotational mobility of the nanomaterial is increased. Precisely, conventional pure LC hybrid composite cell and ultra-thin film nanowires were sandwiched between two ITO–LC cells corresponding

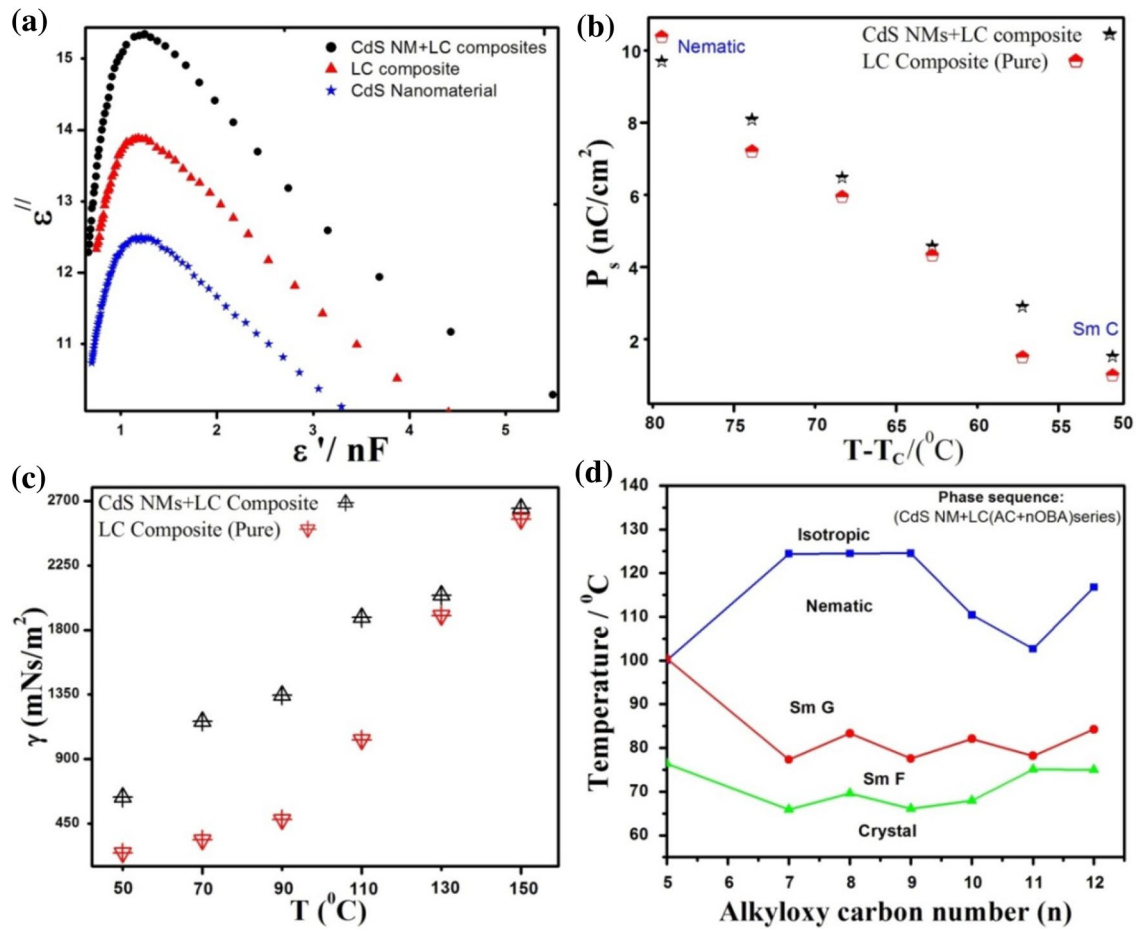


Fig. 6 **a** The variation of dielectric relaxation frequency of dielectric loss magnitude with permittivity is recorded at 50 °C, **b** spontaneous polarization (P_s) against phase transition, **c** temperature dependence rotational viscosity corresponding to pure liquid crystals composite

and CdS nanowires dispersed liquid crystals composite matrix, and **d** phase diagram of (AC+nOBA) homologous series temperature dependence alkyloxy carbon number ($n=5$ and 7)

to the phase diagram of (AC + nOBA) homologous series of liquid crystal as identifies in Fig. 6d.

A detail investigation reveals the following points;

(i) The phase diagram is composed of two phases, e.g. Nematic, Smectic C* and Smectic X*.

(ii) The nematic phase is present in all of the homologues series of liquid crystalline compound of (AC + 5BAO) & (AC + 7BAO).

(iii) In the entire homologous series, in all complexes, the thermal range of the nematic phase is much larger compared to the smectic X* phase.

The capacitance against voltage hysteresis curves of both pure LC compounds and CdS-nanowires incorporated liquid crystalline composites matrix were investigated at 10 kHz frequency range within the applied external bias – 10 to + 10 V by utilization of semiconductor characterization system (Model: SCS-4200), as depicted in Fig. 7a and b. The Preisach model was invoked to fit the C–V curves [20–22]. According to this model,

$$C = C_f + \sum_{(i=1)}^n \frac{P_{si} \cdot \delta_i \cdot A}{\cos h^2 [\delta_i \cdot (V \pm V_{Ci}^{\pm})]} \quad (1)$$

where ‘C’ is the cell capacitance, ‘ C_f ’ is the voltage-independent part of the capacitance, ‘ P_{si} ’ is the spontaneous polarization of all dipoles in the i -th species fully aligned to an external field, ‘A’ is the area of the cell, ‘ V_{Ci} ’ is the coercive voltage at which the electrical polarization of the i -th species vanishes during switching from one orientation to the other, $\delta_i = V_{Ci}^{-1} \log \left\{ \frac{[1 + (P_r/P_{s_i})_i]}{[1 - (P_r/P_{s_i})_i]} \right\}$ is the species-related constant and P_r is the remnant polarization. We have neglected the contribution in the capacitance value from the alignment layer since it is very small. It is very informative from Fig. 7a and b that similar two and four dipolar species from the fitted curves. While, the sharp peak capacitances slightly decreases in case of the LC composite cell as shown in Fig. 7a, with twofold dipolar species were obtained. Interestingly enough, sharp prominent peaks

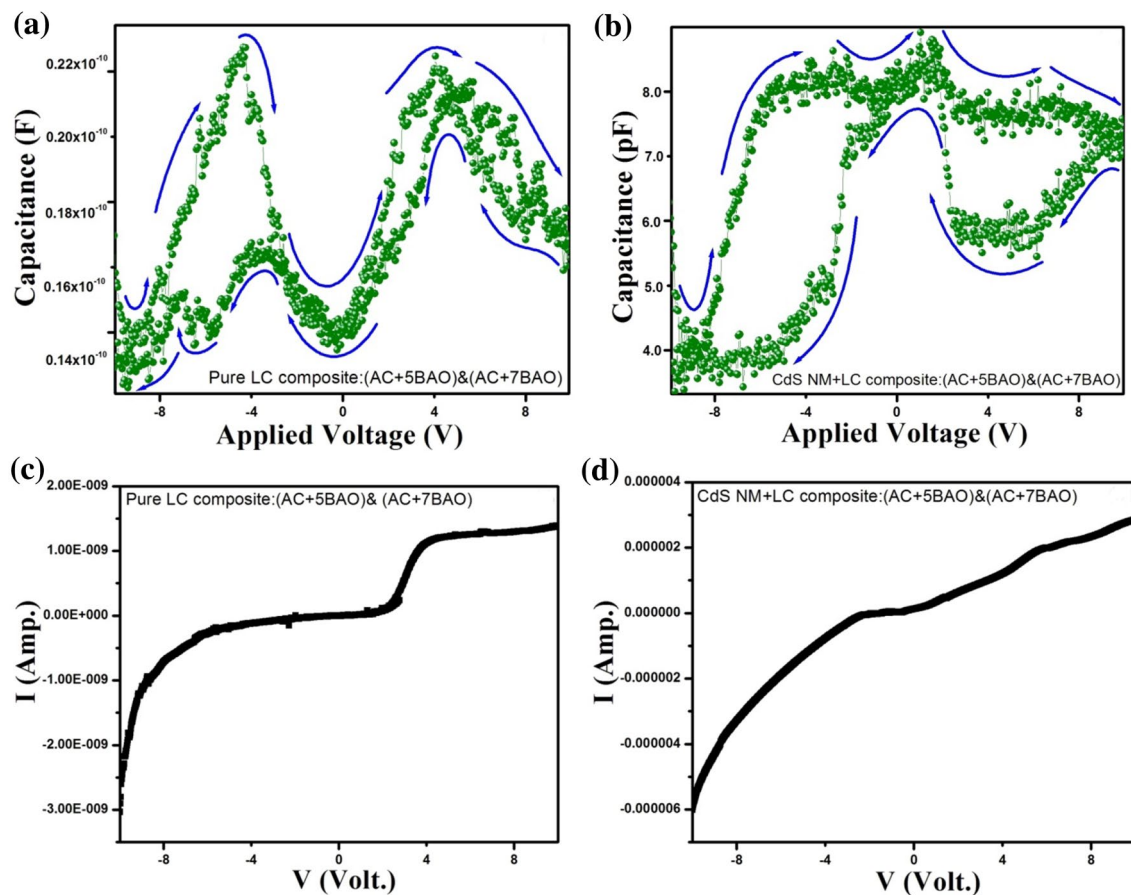


Fig. 7 Capacitance versus voltage hysteresis response of **a** pure liquid crystalline compound, **b** CdS-nanowires dispersed liquid crystalline composite matrix. The forward and reverse bias current sensibility

of applied DC voltage corresponding to **c** pure LC compounds series and, **d** CdS-nanowires dispersed liquid crystalline hybrid composite matrix

were surprisingly vanishes and special signature was carried out by nanowires dispersing into a liquid crystal composite matrix. Remarkable fourfold dipolar species are obtained in Fig. 7b. The bias voltage at which peak capacitance occurs is away from 0 V in the doped cell in comparison with liquid crystalline compound. From the critical analysis, we found that the four dipole species are quite interesting in the CdS-nanowires dispersed LC composite cell, while two dipolar species obtained due to pure LC composite. It suggests that, the inherent dipole moment of CdS nanomaterials interact antiparallely with the surrounding dipolar species to increase the overall spontaneous polarization as well as a high contrast ratio of LC device made of NDLC composite matrix.

Bi-stable DC switching of I–V response characteristics (Model: SCS-4200) as illustrated in the Fig. 7c, and d. However, a very decent remarkable significant behavior evinced i.e. negatively threshold current starts at -9 V, then smoothly increases and saturated within externally applied positive bias resulted due to the pure LC composite cell as shown in Fig. 7c. Interestingly enough, within an applied

positive bias field seems to behave like a ‘conductor \rightarrow insulator’, then ‘insulator \rightarrow conductor’ type. However, those nanostructures are incorporated with LC composite materials responding to an exponentially increasing manner at negative threshold voltage (-9 V) region, while positive threshold starts at $+2.5$ V and increases most linear regular fashion demonstrated in Fig. 7d. Thus, the carrier concentration becomes higher and increasing the conductance.

4 Conclusions

In the proof-of-concept study, we have synthesized high yield CdS nanowires by simple cost-effective surfactant assisted route. In the processes of the nanostructures formation, these bidentate ligand complexes ($[\text{Cd}(\text{en})_2]^{2+}$) play a major role in control of the CdS nanowires nucleation and growth. It may predicted that, the resulting product has a very unique and useful behavior e.g. sulfur powder was dissolved into ethylenediamine (EDA) solution. However, ‘EDA’ acts not only as the nucleophilic attack reagents to release of S^{2-} ions

and the low free Cd^{2+} concentration which is in favor to form molecular template to direct the nucleation as well as oriented growth of CdS nanostructures. The high luminous semiconductor CdS-nanowires having diameter ~ 7 to 10 nm, were obtained and smoothly deposited with hydrogen bonded liquid crystalline materials. The special chemical structure can lead to the formation of new Sm X* phase appeared with temperature transition due to HBLCs. A new smectic ordering labeled as ‘Sm G*’, which is sandwiched between traditional ‘nematic (N)’ and convectional ‘Sm C*’ phases reveals a remarkable investigation. The most significant advantage of this novel approaches exploring surface stabilized sensible switching device response through C–V and I–V characteristics. The syntheses of hydrogen-bonded composite LCs are relatively easier than that of conventional LCs and also the influence of nanomaterials have the potential for developing optical and electrical properties. Based on C–V analysis we may predict the antiparallel dipole–dipole interaction of the semiconductor hybrid complex materials deposited into LC host structures with the dipole species of the FLC reduces the ‘spontaneous polarization (P_s)’ in the doped cell. The higher local electric field in the HBLC/CdS-nanocomposite improves the response to an external electric field. Moreover, bi-stable DC switching appeared (Conductor \rightarrow Insulator), so the fluctuation/stability of current also observed due to influence of CdS nanostructures doped LC and undoped LC materials, compared with ITO–LC hybrid composite cell. Overall an unique expansion of nanostructures homogenous dispersion strategy has exhibited a great potential significance. As well as controllable syntheses of others nanomaterials technologically important, which will provide new insights emerging applications and help to solve many scientific issues.

Acknowledgements The author Dr. Kaushik Pal is grateful to his associate colleagues & doctoral research scholars at *Wuhan University, China*. Especially, Dr. Pal, owe to his sincere thanks to associate colleagues included Bachelor/Masters/Ph.D. students, spectroscopy/electron microscopy operators, as well as entire team of research scholars are also gratefully acknowledged during “Visiting Scientist” associate ship at *CNU, South Korea*. We are honor to Prof. Mohan’s co-workers of the *Liquid Crystals Research Laboratory at Bannari Amman Institute of Technology, Sathyamangalam* encouraging liquid crystal preparation. Sincere ‘Thanks’ goes to Dean (Research), at *BIHER Chennai (India)* for providing Dr. Pal to develop the excellence of research foundation associated with existing Nanotechnology laboratory. The research scholars from Niel University, Egypt are gratefully acknowledged for giving scopes to develop research ideas and scientific innovations. The author Mohamed Abd Elkodous is also grateful to Dean (Research) for giving research friendly scopes at *Nile University, Egypt*.

Compliance with ethical standards

Conflict of interest All the authors have declared that, there is no conflict of interest regarding the contribution to the feature article publication.

References

1. Y. Xia et al., One-dimensional nanostructures: synthesis, characterization, and applications. *Adv. Mater.* **15**(5), 353–389 (2003)
2. A.L. Prieto et al., Electrodeposition of ordered Bi_2Te_3 nanowire arrays. *J. Am. Chem. Soc.* **123**(29), 7160–7161 (2001)
3. L. Brus, Quantum crystallites and nonlinear optics. *Appl. Phys. A* **53**(6), 465–474 (1991)
4. H. Weller, Colloidal semiconductor q-particles: chemistry in the transition region between solid state and molecules. *Angew. Chem. Int. Ed.* **32**(1), 41–53 (1993)
5. K. Pal et al., A facile strategy for the fabrication of uniform CdS nanowires with high yield and its controlled morphological growth with the assistance of PEG in hydrothermal route. *Appl. Surf. Sci.* **258**(1), 163–168 (2011)
6. K. Pal et al., Synthetic strategy of porous ZnO and CdS nanostructures doped ferroelectric liquid crystal and its optical behavior. *J. Mol. Struct.* **1035**, 76–82 (2013)
7. K. Pal et al., Dielectric and I–V characteristics of high luminous CdS nanostructures with confined geometrical growth. *J. Mol. Struct.* **1041**, 16–22 (2013)
8. K. Pal et al., Switching of ferroelectric liquid crystal doped with cetyltrimethylammonium bromide-assisted CdS nanostructures. *Nanotechnology* **24**(12), 125702 (2013)
9. K. Pal et al., Ultraviolet visible spectroscopy of CdS nano-wires doped ferroelectric liquid crystal. *J. Mol. Liq.* **164**(3), 233–238 (2011)
10. K. Pal et al., Temperature variation dielectric behavior of TiO_2 nanocabbages and doped W-182 (AFLC). *J. Lumin.* **136**, 278–284 (2013)
11. K. Pal et al., Optical and electrical investigation of ZnO nano-wire array to micro-flower from hierarchical nano-rose structures. *J. Nanosci. Nanotechnol.* **16**(1), 400–409 (2016)
12. K. Pal et al., Influence of ZnO nanostructures in liquid crystal interfaces for bistable switching applications. *Appl. Surf. Sci.* **357**, 1499–1510 (2015)
13. K. Pal et al., Design, synthesis and application of hydrogen bonded smectic liquid crystal matrix encapsulated ZnO nanospikes. *J. Mater. Chem. C* **3**(45), 11907–11917 (2015)
14. G.C. Pimentel, A. McClellan, Hydrogen bonding. *Annu. Rev. Phys. Chem.* **22**(1), 347–385 (1971)
15. T. Elsaesser, H. Becker, *Ultrafast Hydrogen Bonding Dynamics and Proton Transfer Processes in the Condensed Phase*, vol. 23 (Springer, New York, 2013)
16. I. Gitsov, K. Wooley, J. Fréchet, *Angew. Chem. Int. Ed.* **31**, 1200 (1992)
17. I. Gitsov, K.L. Wooley, C.J. Hawker, P.T. Ivanova, J.M.J. Fréchet, *Macromolecules* **26**, 5621 (1993)
18. L. Yu, Hydrogen bond-induced ferroelectric liquid crystals. *Liq. Cryst.* **14**(5), 1303–1309 (1993)
19. K. Pal et al., Switchable, self-assembled CdS nanomaterials embedded in liquid crystal cell for high performance static memory device. *Mater. Lett.* **169**, 37–41 (2016)
20. S. Miller et al., Modeling ferroelectric capacitor switching with asymmetric nonperiodic input signals and arbitrary initial conditions. *J. Appl. Phys.* **70**(5), 2849–2860 (1991)
21. S. Miller et al., Device modeling of ferroelectric capacitors. *J. Appl. Phys.* **68**(12), 6463–6471 (1990)
22. P. Yang et al., Electrical properties of $\text{SrBi}_2\text{Ta}_2\text{O}_9$ ferroelectric thin films at low temperature. *Appl. Phys. Lett.* **81**(24), 4583–4585 (2002)